ON THE PREDICTION OF MULTIGRID EFFICIENCY
THROUGH LOCAL MODE ANALYSIS

S22-64

197682

p.-11

R.V. Wilson
Department of Mechanical Engineering and Mechanics
Old Dominion University
Norfolk, Virginia

ABSTRACT

A single grid local mode analysis is used to predict the smoothing properties of numerical schemes for solving the Navier-Stokes equations with factorization based on Stone's Strongly Implicit Method. Four difference approximations for the convection terms are considered, namely, hybrid, central, second-order upwind, and third-order upwind. Smoothing factors from the analysis are compared with practical convergence factors in a multigrid method for flow over a backward facing step and it is found that the local mode analysis correctly predicts the effects of Reynolds number and higher-order schemes.

1 INTRODUCTION

The successful use of multigrid methods to accelerate convergence rates is dependent on the ability of the numerical algorithm to dampen high frequency error components since these components cannot be resolved on coarser grids. High frequency components have short coupling ranges; therefore, their smoothing is a localized process meaning that only one isolated computational stencil need be analyzed and the effect of boundaries can be neglected. This is the approach of local mode analysis for the prediction of smoothing properties which was first introduced by Brandt [1] for various partial differential equations and numerical algorithms. Shaw and Sivaloganathan [2] extended this analysis to the SIMPLE pressure correction algorithm using alternating direction implicit (ADI) relaxation for the solution of the algebraic system of equations for varying Reynolds numbers and under-relaxation factors. Convection terms were approximated using a hybrid of first-order upwind and second-order central differencing.

The present paper uses local mode analysis to predict the smoothing properties of numerical algorithms for calculation of two-dimensional recirculating flows using higher-order difference schemes for convection terms introduced via deferred correction and Stone's Strongly Implicit Method for factorization of the resulting system of algebraic equations. Reynolds number and higher-order convection approximation effects are addressed and compared to multigrid results for laminar flow over a backward facing step.

2 THEORETICAL ANALYSIS

2.1 Governing equations

The equations governing steady, two-dimensional, incompressible flow can be written as:

$$\frac{\partial}{\partial x}(\rho u) + \frac{\partial}{\partial y}(\rho v) = 0 \tag{1}$$

$$\frac{\partial}{\partial x}(\rho u^2) + \frac{\partial}{\partial y}(\rho uv) = -\frac{\partial p}{\partial x} + \mu\left(\frac{\partial^2 u}{\partial x^2} + \frac{\partial^2 u}{\partial y^2}\right) \tag{2}$$

$$\frac{\partial}{\partial x}(\rho uv) + \frac{\partial}{\partial y}(\rho v^2) = -\frac{\partial p}{\partial y} + \mu\left(\frac{\partial^2 v}{\partial x^2} + \frac{\partial^2 v}{\partial y^2}\right) \tag{3}$$

where u and v are the velocity components in the x and y directions, respectively, p is the pressure, μ is the absolute viscosity, and ρ is the density. Equations (1) - (3) represent the conservation of mass and momentum in the x and y directions, respectively.

The solution sequence is a predictor-corrector method which follows the SIMPLE algorithm of Patankar and Spalding [3]. Factorization of the system of equations is based on Stone's Strongly Implicit Method. The flow geometry and boundary conditions are shown in Figure 1.

The governing equations are discretized by integrating over a set of three staggered control volumes and the locations of variables are shown in Figure 2. The central control volume is for the pressure. Equation (2) can be discretized by integrating over the left-shifted control volume for the u component of velocity. This leads to:

$$a_P u_P = a_E u_E + a_W u_W + a_N u_N + a_S u_S + a_{EE} u_{EE} + a_{WW} u_{WW} + a_{NN} u_{NN} + a_{SS} u_{SS}$$

$$-\frac{(p_P - p_W)}{h_x} + \left(\frac{\mu_o}{h_x h_y}\right)(v_N - v_{NW} + v_W - v_P) + \frac{\mu_o}{h_x^2}(u_E - 2u_P + u_W) \tag{4}$$

Equation (3) is discretized by integrating over the bottom-shifted control volume for the v component of velocity:

$$a_P v_P = a_E v_E + a_W v_W + a_N v_N + a_S v_S + a_{EE} v_{EE} + a_{WW} v_{WW} + a_{NN} v_{NN} + a_{SS} v_{SS}$$

$$-\frac{(p_P - p_S)}{h_y} + \left(\frac{\mu_o}{h_x h_y}\right)(u_E - u_{SE} + u_S - u_P) + \frac{\mu_o}{h_y^2}(v_N - 2v_P + v_S) \tag{5}$$

where the a_i coefficients contain convection and diffusion terms, the subscripts of u, v, and p refer to the location of the variables (see figure 2), h_x and h_y are the grid spacing in the x and y directions, respectively, and μ_o is the absolute viscosity of the fluid, assumed constant.

2.2 Approximation of convection terms

The a_i coefficients in equations (4) and (5) are dependent on the approximation used for the convec-

tion terms. The present analysis investigates the hybrid, central, second-order upwind (2nd OU), and third-order upwind (3rd OU) approximation schemes.

The coefficients for the hybrid scheme have the following form:

$$a_E = max\{0, \frac{\mu_o}{h_x^2} - \frac{|\rho u_o|}{2h_x}\} + max\{-\frac{\rho u_o}{h_x}, 0\}$$ (6)

$$a_W = max\{0, \frac{\mu_o}{h_x^2} - \frac{|\rho u_o|}{2h_x}\} + max\{\frac{\rho u_o}{h_x}, 0\}$$ (7)

$$a_N = max\{0, \frac{\mu_o}{h_y^2} - \frac{|\rho v_o|}{2h_y}\} + max\{-\frac{\rho v_o}{h_y}, 0\}$$ (8)

$$a_S = max\{0, \frac{\mu_o}{h_y^2} - \frac{|\rho v_o|}{2h_y}\} + max\{\frac{\rho v_o}{h_y}, 0\}$$ (9)

$$a_{EE} = a_{WW} = a_{NN} = a_{SS} = 0$$ (10)

$$a_P = \Sigma a_i$$ (11)

where the sum for a_P is taken over the a coefficients, u_o and v_o are the frozen velocity components due to the linearization of equations (2) and (3), the $max\{a,b\}$ operator selects the maximum of the arguments a and b, and $|\ |$ represents the absolute value.

The coefficients for the higher-order schemes have the following general form:

$$a_E = \frac{\mu_o}{h_x^2} - \frac{\rho u_o}{2h_x} + f_1\left[max\{\frac{\rho u_o}{h_x}, 0\} + max\{-\frac{\rho u_o}{h_x}, 0\}\right] + f_2 max\{-\frac{\rho u_o}{h_x}, 0\}$$ (12)

$$a_W = \frac{\mu_o}{h_x^2} + \frac{\rho u_o}{2h_x} + f_1\left[max\{\frac{\rho u_o}{h_x}, 0\} + max\{-\frac{\rho u_o}{h_x}, 0\}\right] + f_2 max\{\frac{\rho u_o}{h_x}, 0\}$$ (13)

$$a_N = \frac{\mu_o}{h_y^2} - \frac{\rho v_o}{2h_y} + f_1\left[max\{\frac{\rho v_o}{h_y}, 0\} + max\{-\frac{\rho v_o}{h_y}, 0\}\right] + f_2 max\{-\frac{\rho v_o}{h_y}, 0\}$$ (14)

$$a_S = \frac{\mu_o}{h_y^2} + \frac{\rho v_o}{2h_y} + f_1\left[max\{\frac{\rho v_o}{h_y}, 0\} + max\{-\frac{\rho v_o}{h_y}, 0\}\right] + f_2 max\{\frac{\rho v_o}{h_y}, 0\}$$ (15)

$$a_{EE} = -f_1 max\{-\frac{\rho u_o}{h_x}, 0\}$$ (16)

$$a_{WW} = -f_1 max\{\frac{\rho u_o}{h_x}, 0\}$$ (17)

$$a_{NN} = -f_1 max\{-\frac{\rho v_o}{h_y}, 0\}$$ (18)

$$a_{SS} = -f_1 max\{\frac{\rho v_o}{h_y}, 0\}$$ (19)

$$a_P = \Sigma a_i$$ (20)

The values of f_1 and f_2 depend on the higher-order method to be used. For central differencing, $f_1=f_2$ = 0, for 2nd OU differencing, f_1 = 1/2 and f_2 = 1, and for 3rd OU differencing, f_1 = 1/8 and f_2 = 1/4.

2.3 Local mode analysis

The Strongly Implicit Method (SIP) by Stone [4] solves the algebraic equations shown in equations (4) and (5) in a fully implicit manner. All variables are treated as unknowns, as opposed to line-relaxation methods which consider only lines of constant x or y as unknowns while sweeping through the computational domain. In the local mode analysis outlined below, the variables that are updated at the end of a relaxation sweep will be denoted by a dot over the variable, such as $\dot{u}_P$, while those from the beginning of the relaxation sweep or those unchanged by the current relaxation sweep will be written as above, such as u_P. Higher-order approximations for the convection terms are introduced via deferred correction (see Khosla and Rubin [5]). In this procedure, the a_i coefficients are calculated initially using equations (6) - (11) for the hybrid scheme. As the solution proceeds, the higher-order scheme is slowly introduced via corrections to the source terms. At the end when the solution is fully converged, the coefficients are effectively those of the higher-order scheme outlined in equations (12) - (20). The base hybrid coefficients will be denoted by an additional subscript h, such as $a_P|_h$, while the higher-order coefficients will not have an additional subscript and will be written as above, such as a_P.

The relaxation of equation (4) (the discretized x momentum equation), with under-relaxation and deferred correction can be written as:

$$a_P|_h \dot{u}_P = a_P|_h u_P + r_m \left(a_E|_h \dot{u}_E + a_W|_h \dot{u}_W + a_N|_h \dot{u}_N + a_S|_h \dot{u}_S - a_P|_h u_P \right)$$

$$+ r_m \left\{ \frac{-(p_P - p_W)}{h_x} + \left(\frac{\mu_o}{h_x h_y} \right)(v_N - v_{NW} + v_W - v_P) + \frac{\mu_o}{h_x^2}(\dot{u}_E - 2\dot{u}_P + \dot{u}_W) \right\}$$

$$+ r_1 r_m [(a_E - a_E|_h)(u_E - u_P) + (a_W - a_W|_h)(u_W - u_P) + (a_N - a_N|_h)(u_N - u_P) + (a_S - a_S|_h)(u_S - u_P)$$

$$+ a_{EE}(u_{EE} - u_P) + a_{WW}(u_{WW} - u_P) + a_{NN}(u_{NN} - u_P) + a_{SS}(u_{SS} - u_P)] \quad (21)$$

where r_m is the under-relaxation factor for the x and y momentum equations, r_1 is the relaxation factor for introducing higher-order coefficients and is set to unity for the analysis. The exact solution for U, V, and P also satisfies equation (21). If an equation written with the exact solution for U, V, and P is subtracted from equation (21), which is written in terms of the approximate solution, u, v, and p, the error in the solution can be introduced. The error has components defined as; $\varepsilon^u = U - u$, $\varepsilon^v = V - v$, and $\varepsilon^p = P - p$.

Equation (21) written in terms of the error becomes:

$$a_P|_h \dot{\varepsilon}^u_P = a_P|_h \varepsilon^u_P + r_m \left(a_E|_h \dot{\varepsilon}^u_E + a_W|_h \dot{\varepsilon}^u_W + a_N|_h \dot{\varepsilon}^u_N + a_S|_h \dot{\varepsilon}^u_S - a_P|_h \varepsilon^u_P \right)$$

$$+ r_m \left\{ \frac{-(\varepsilon^p_P - \varepsilon^p_W)}{h_x} + \left(\frac{\mu_o}{h_x h_y} \right)(\varepsilon^v_N - \varepsilon^v_{NW} + \varepsilon^v_W - \varepsilon^v_P) + \frac{\mu_o}{h_x^2}(\dot{\varepsilon}^u_E - 2\dot{\varepsilon}^u_P + \dot{\varepsilon}^u_W) \right\}$$

$$+ r_1 r_m [(a_E - a_E|_h)(\varepsilon^u_E - \varepsilon^u_P) + (a_W - a_W|_h)(\varepsilon^u_W - \varepsilon^u_P) + (a_N - a_N|_h)(\varepsilon^u_N - \varepsilon^u_P) + (a_S - a_S|_h)(\varepsilon^u_S - \varepsilon^u_P)$$

$$+ a_{EE}(\varepsilon^u_{EE} - \varepsilon^u_P) + a_{WW}(\varepsilon^u_{WW} - \varepsilon^u_P) + a_{NN}(\varepsilon^u_{NN} - \varepsilon^u_P) + a_{SS}(\varepsilon^u_{SS} - \varepsilon^u_P)] \quad (22)$$

Since the continuous governing equations (1) - (3) have been linearized during the discretization, a single Fourier component of the error can be considered as:

$$\varepsilon^u_P = \alpha^u_\theta e^{i\left[\theta_1\frac{x}{h_x}+\theta_2\frac{y}{h_y}\right]}$$

$$\varepsilon^u_W = \alpha^u_\theta e^{i\left[\theta_1\frac{(x-h_x)}{h_x}+\theta_2\frac{y}{h_y}\right]}$$

$$\varepsilon^u_S = \alpha^u_\theta e^{i\left[\theta_1\frac{x}{h_x}+\theta_2\frac{(y-h_y)}{h_y}\right]} \tag{23}$$

where $i = \sqrt{-1}$, Θ_1 and Θ_2 are the components of the phase angle vector, α_θ, which is the error amplitude of the single Fourier mode Θ_1, Θ_2. Similar expressions exist for other grid points to the east and north and for the variables v and p. Substituting the single Fourier modes into equation (22) and dividing through by $e^{i[\theta_1 x/h_x + \theta_2 y/h_y]}$, equation (22) becomes:

$$\dot{\alpha}^u_\theta \left\{ a_P|_h - r_m \left(a_E|_h e^{i\theta_1} + a_W|_h e^{-i\theta_1} + a_N|_h e^{i\theta_2} + a_S|_h e^{-i\theta_2} - \frac{4\mu_o s_1^2}{h_x^2} \right) \right\} =$$

$$\alpha^u_\theta \{ a_P|_h (1-r_m) + r_1 r_m [(a_E - a_E|_h) (e^{i\theta_1} - 1) + (a_W - a_W|_h) (e^{-i\theta_1} - 1) + (a_N - a_N|_h) (e^{i\theta_2} - 1)$$

$$+ (a_S - a_S|_h) (e^{-i\theta_2} - 1) + a_{EE}(e^{2i\theta_1} - 1) + a_{WW}(e^{-2i\theta_1} - 1) + a_{NN}(e^{2i\theta_2} - 1) + a_{SS}(e^{-2i\theta_2} - 1)] \}$$

$$- \frac{4 r_m \mu_o s_1 s_2}{h_x h_y} \alpha^v_\theta - \frac{2 r_m s_1 i}{h_x} \alpha^p_\theta \tag{24}$$

where: $s_1 = \sin(\theta_1/2)$
$s_2 = \sin(\theta_2/2)$

Equation (24) can be written in a more compact form, if the following variables are defined:

$$\eta^u = a_P|_h - r_m \left(a_E|_h e^{i\theta_1} + a_W|_h e^{-i\theta_1} + a_N|_h e^{i\theta_2} + a_S|_h e^{-i\theta_2} - \frac{4\mu_o s_1^2}{h_x^2} \right)$$

$$\nu = a_P|_h (1-r_m) + r_1 r_m [(a_E - a_E|_h) (e^{i\theta_1} - 1) + (a_W - a_W|_h) (e^{-i\theta_1} - 1) + (a_N - a_N|_h) (e^{i\theta_2} - 1)$$

$$+ (a_S - a_S|_h) (e^{-i\theta_2} - 1) + a_{EE}(e^{2i\theta_1} - 1) + a_{WW}(e^{-2i\theta_1} - 1) + a_{NN}(e^{2i\theta_2} - 1) + a_{SS}(e^{-2i\theta_2} - 1)]$$

$$\varphi = \frac{4 r_m \mu_o s_1 s_2}{h_x h_y}$$

$$\zeta^u = \frac{2 r_m s_1 i}{h_x}$$

Equation (24) can then be written as:

$$\dot{\alpha}^u_\theta = \frac{1}{\eta^u} (\nu \alpha^u_\theta - \varphi \alpha^v_\theta - \zeta^u \alpha^p_\theta) \tag{25}$$

Following the same procedure for equation (5) (the discretized y momentum equation) yields:

$$\dot{\alpha}_\theta^v = \frac{1}{\eta^v}(v\alpha_\theta^v - \varphi\dot{\alpha}_\theta^u - \zeta^v\alpha_\theta^p) \tag{26}$$

where:

$$\eta^v = a_P|_h - r_m\left(a_E|_h e^{i\theta_1} + a_W|_h e^{-i\theta_1} + a_N|_h e^{i\theta_2} + a_S|_h e^{-i\theta_2} - \frac{4\mu_o s_2^2}{h_y^2}\right)$$

$$\zeta^v = \frac{2r_m s_2 i}{h_y}$$

Equations (25) and (26) can be combined to give the amplification matrix A_1 for the complete operation. This yields:

$$\begin{bmatrix} \dot{\alpha}_\theta^u \\ \dot{\alpha}_\theta^v \\ \dot{\alpha}_\theta^p \end{bmatrix} = \begin{bmatrix} \left\{\dfrac{v}{\eta^u}\right\} & \left\{\dfrac{-\varphi}{\eta^u}\right\} & \left\{\dfrac{-\zeta^u}{\eta^u}\right\} \\ \left\{\dfrac{-\varphi v}{\eta^u\eta^v}\right\} & \left\{\dfrac{\varphi^2}{\eta^u\eta^v} + \dfrac{v}{\eta^v}\right\} & \left\{\dfrac{\varphi\zeta^u}{\eta^u\eta^v} - \dfrac{\zeta^v}{\eta^v}\right\} \\ 0 & 0 & 1 \end{bmatrix} \begin{bmatrix} \alpha_\theta^u \\ \alpha_\theta^v \\ \alpha_\theta^p \end{bmatrix}$$

In compact form:

$$\dot{\alpha}_\theta = A_1\alpha_\theta \tag{27}$$

Equation (27) yields the amplification matrix defining how the amplitude of the Fourier mode, with phase angles θ_1 and θ_2, is amplified during relaxation of the x and y momentum equations.

The SIMPLE pressure correction of Patankar and Spalding [3] follows the relaxation of the x and y momentum equations. A single dot over a variable will denote a value at the completion of the relaxation of the x and y momentum equations. A double dot over a variable will denote a value at the completion of the pressure correction. The variables u, v, and p are corrected following Shaw and Sivaloganathan [2]:

$$\ddot{u}_P = \dot{u}_P - \frac{r_{uv}}{a_P^u h_x}(\delta p_P - \delta p_W) \tag{28}$$

$$\ddot{v}_P = \dot{v}_P - \frac{r_{uv}}{a_P^v h_y}(\delta p_P - \delta p_S) \tag{29}$$

$$\ddot{p}_P = \dot{p}_P + r_p\delta p_P \tag{30}$$

where r_{uv} is the relaxation factor for correcting u and v velocities and r_p is the relaxation factor for updating pressure. The value δp is a pressure increment such that the velocity field $\ddot{u}$ and $\ddot{v}$ will satisfy conservation of mass. It is obtained by discretizing equation (3) and substituting for the velocities and corrections given in equations (28) - (30). This yields an equation for the pressure correction:

$$d^p{}_P\delta p_P = d^p{}_N\delta p_N + d^p{}_S\delta p_S + d^p{}_E\delta p_E + d^p{}_W\delta p_W - \frac{1}{h_x}(\dot{u}_E - \dot{u}_P) - \frac{1}{h_y}(\dot{v}_N - \dot{v}_P) \tag{31}$$

where:
$$d^p_N = \frac{1}{a^v_p h^2_y} = d^p_S$$

$$d^p_E = \frac{1}{a^u_p h^2_x} = d^p_W$$

$$d^p_P = d^p_N + d^p_S + d^p_E + d^p_W$$

Equations (28) - (31) can be written in compact form as:

$$\ddot{u}_P = \dot{u}_P - \frac{r_{uv}}{a^u_P}\delta^x_h \delta p_h \tag{32}$$

$$\ddot{v}_P = \dot{v}_P - \frac{r_{uv}}{a^v_P}\delta^y_h \delta p_h \tag{33}$$

$$\ddot{p}_h = \dot{p}_h + r_p \delta p_h \tag{34}$$

$$P_h \delta p_h = \delta^x_h \dot{u}_h + \delta^y_h \dot{v}_h \tag{35}$$

If equation (35) is solved for δp_h and used in equation (32)-(34):

$$\ddot{u}_h = \dot{u}_h - \frac{r_{uv}}{a^u_P}\delta^x_h P^{-1}_h (\delta^x_h \dot{u}_h + \delta^y_h \dot{v}_h) \tag{36}$$

$$\ddot{v}_h = \dot{v}_h - \frac{r_{uv}}{a^v_P}\delta^y_h P^{-1}_h (\delta^x_h \dot{u}_h + \delta^y_h \dot{v}_h) \tag{37}$$

$$\ddot{p}_h = \dot{p}_h + r_p P^{-1}_h (\delta^x_h \dot{u}_h + \delta^y_h \dot{v}_h) \tag{38}$$

This assumes that the pressure correction equation has been solved exactly. As before, the error is introduced by writing equations (36)-(38) using the exact solution and then subtracting the result from equations (36)-(38) respectively. The errors become:

$$\ddot{\varepsilon}^u_h = \dot{\varepsilon}^u_h - \frac{r_{uv}}{a^u_P}\delta^x_h P^{-1}_h (\delta^x_h \dot{\varepsilon}^u_h + \delta^y_h \dot{\varepsilon}^v_h) \tag{39}$$

$$\ddot{\varepsilon}^v_h = \dot{\varepsilon}^v_h - \frac{r_{uv}}{a^v_P}\delta^y_h P^{-1}_h (\delta^x_h \dot{\varepsilon}^u_h + \delta^y_h \dot{\varepsilon}^v_h) \tag{40}$$

$$\ddot{\varepsilon}^p_h = \dot{\varepsilon}^p_h + r_p P^{-1}_h (\delta^x_h \dot{\varepsilon}^u_h + \delta^y_h \dot{\varepsilon}^v_h) \tag{41}$$

The Fourier components of the error can be substituted as before to give the A_2 amplification matrix which governs the amplification of errors during the pressure correction phase:

$$\begin{bmatrix} \ddot{\alpha}^u_\theta \\ \ddot{\alpha}^v_\theta \\ \ddot{\alpha}^p_\theta \end{bmatrix} = \begin{bmatrix} \left\{1 + \frac{4r_{uv}s^2_1}{a^u_P P_h h^2_x}\right\} & \left\{\frac{4r_{uv}s_1 s_2}{a^u_P P_h h_x h_y}\right\} & 0 \\ \left\{\frac{4r_{uv}s_1 s_2}{a^v_P P_h h_x h_y}\right\} & \left\{1 + \frac{4r_{uv}s^2_2}{a^v_P P_h h^2_y}\right\} & 0 \\ \left\{\frac{2r_p s_1}{P_h h_x}i\right\} & \left\{\frac{2r_p s_2}{P_h h_y}i\right\} & 1 \end{bmatrix} \begin{bmatrix} \dot{\alpha}^u_\theta \\ \dot{\alpha}^v_\theta \\ \dot{\alpha}^p_\theta \end{bmatrix}$$

In compact form:

$$\ddot{\alpha}_\theta = A_2 \dot{\alpha}_\theta \qquad (42)$$

where: $\quad \hat{P}_h = a_E^p e^{i\theta_1} + a_W^p e^{-i\theta_1} + a_N^p e^{i\theta_2} + a_S^p e^{-i\theta_2} - a_P^p$

Equation (42) gives the amplification matrix defining how the amplitude of the Fourier mode with phase angles θ_1 and θ_2 is amplified during the pressure correction phase of the algorithm. The amplification matrix for relaxation of the x and y momentum equations and the pressure correction is obtained by combining equation (27) and (42) as:

$$\ddot{\alpha}_\theta = A_2 A_1 \alpha_\theta = A \alpha_\theta \qquad (43)$$

2.4 Smoothing factor

The smoothing factor is a measure of the worst reduction of the high frequency error components for one complete relaxation sweep. It is calculated as the largest eigenvalue of the amplification matrix A given by equation (43) for the Fourier modes θ_1 and θ_2 in the high frequency range defined as: $\pi/2 \leq |\Theta_1| \leq \pi$ and $\pi/2 \leq |\Theta_2| \leq \pi$.

3 RESULTS

To test the predictive capability of the LMA presented in Section 2, flow over a backward facing step (BFS) was computed using a multigrid code based on the FAS-FMG (full approximation storage - full multi-grid) algorithm proposed by Brandt [1]. Higher-order schemes were introduced through deferred correction only on the finest of three grids with constant grid spacing in the x and y directions. The grid sizes from coarsest to finest grid are, $n_x \times n_y = 66 \times 18$, 130×34, and 258×66, where n_x is the number of grid points in the x direction and n_y is the number of grid points in the y direction. Smoothing properties on the two coarser grids are identical for the four schemes since hybrid coefficients were used on these grids. Local mode analysis was used to estimate the smoothing factor on the finest grid and this result was compared to the number of work units to reach convergence for the multigrid result. The work units (WU) and convergence factor (CF) are indicators of the smoothing properties of the algorithm and numerical scheme. The work units for a two-dimensional problem with grid refinement in the x and y directions are defined as:

$$WU = \sum_{i=1}^{N} \tau_i 2^{2(i-N)} \qquad (44)$$

where τ_i is the number of iterations on the ith grid at convergence, $i = 1$ for the coarsest grid, and $i = N$ for the finest grid. The convergence factor is defined as:

$$CF = (r_f/r_i)^{1/\Delta WU} \qquad (45)$$

where r_i is the initial norm of the residuals of the x momentum, y momentum, and pressure correction equation on the fine grid, r_f is the norm of the residuals at convergence on the fine grid, and ΔWU is the

change in work units on the fine grid.

The BFS flow was solved for Reynolds numbers (based on the upstream channel height) of 100, 250, and 400 using the hybrid, central, 2nd OU, and 3rd OU schemes. The work units for convergence and convergence factors are shown in Table 1. The smoothing factors were calculated for conditions identical to the finest grid of the multigrid results (the same grid spacing, relaxation factors, density, etc..). The only parameter varied was the frozen velocity components needed to calculate the coefficients in equations (6) - (20) of the various schemes. The maximum velocity components provide an upper bound for the smoothing factor which will dominate the smoothing properties since it was found that as the cell-Reynolds number (Reynolds number with the length scale based on the grid spacing) approaches zero, corresponding to regions where the velocity approaches zero, the smoothing factor also decreases. An estimate of the maximum velocity components for the BFS flow is $u_o = 1.5$ at $y = 0.25$ at the inlet, and $v_o = 0.15$ near recirculation regions. Three principal flow directions are considered with velocity components given by: $u_o, v_o = (0, 0.15), (1.5, 0.15),$ and $(1.5, 0)$. The SIP method exhibits symmetry about the x and y axis so that other flow direction results can be obtained from the three principal flow direction results. For example, the smoothing factors for $u_o, v_o = (-1.5, 0.15), (-1.5, -0.15),$ and $(1.5, -0.15)$ are equal to the smoothing factor for $u_o, v_o = (1.5, 0.15)$. The smoothing factor is then defined as the largest eigenvalue of the amplification matrix A, defined by equation (43), for the three flow directions while restricting the phase angles to the high frequency range. Results from the three principal flow directions show that the flow direction $u_o, v_o = (1.5, 0.15)$ produced the largest eigenvalue for all Reynolds numbers, and thus the smoothing factor was based on this flow direction. The computed smoothing factors are shown in Table 2.

The results of Table 2 show that as the cell-Reynolds number in the LMA is increased, the smoothing factor also increases for the four schemes. More work units will be required to smooth the high frequency error components. The results in Table 1 show that the work units increase and the convergence factor deteriorates as the Reynolds number increases. For the $Re = 100$ results, the LMA predicts that the smoothing properties of the hybrid, central, and 3rd OU will be virtually identical while that of the 2nd OU will be slightly worse. The multigrid results confirm this prediction. For the $Re = 250$ and 400 results, the LMA predicts that the hybrid difference scheme will have the best smoothing properties while the central difference scheme will have the worst, and the 2nd OU and 3rd OU difference schemes should be similar with the 3rd OU difference scheme slightly better. The multigrid results confirm these predictions with the exception being that the 2nd OU difference scheme results converged in slightly less number of work units when compared to the 3rd OU difference scheme. Their convergence factors are similar.

Table I: Work Units/Convergence Factors of Multigrid Results

Difference Scheme	$Re = 100$	$Re = 250$	$Re = 400$
Hybrid	59/0.868	137/0.930	321/0.981
Central	58/0.873	166/0.964	569/0.993
2nd OU	63/0.891	148/0.952	421/0.988
3rd OU	58/0.875	152/0.956	428/0.988

Table II: Smoothing Factors from Local Mode Analysis

Difference Scheme	$Re = 100$	$Re = 250$	$Re = 400$
Hybrid	0.902	0.924	0.931
Central	0.910	0.950	0.968
2nd OU	0.931	0.946	0.950
3rd OU	0.899	0.926	0.935
$Re_{\Delta x}/Re_{\Delta y}$	11.72/0.47	29.30/1.18	46.88/1.88

CONCLUSION

Local mode analysis was performed using four schemes for the approximation of convection terms: hybrid, central, second-order upwind, and third-order upwind, over a range of cell-Reynolds numbers. The smoothing factors from this analysis were compared with actual multigrid results for flow over a backward facing step to test the predictive capability of local mode analysis. It was found that this analysis is useful in predicting the smoothing properties of the four schemes along with the effect of flow Reynolds number. This analysis could be extended to predict optimum relaxation factors, grid aspect ratios, and other solution algorithms.

ACKNOWLEDGEMENTS

REFERENCES

1. Brandt, A.: Multi-level Adaptive Solutions to Boundary-Value Problems, *Math. Comput.*, vol. 31, no. 138, 1977, pp. 330-390.

2. Shaw, G.J.; and Sivaloganathan, S.: On the Smoothing Properties of the SIMPLE Pressure-Correction Algorithm, *Int. J. Numer. Methods Fluids*, vol 8, 1988, pp. 441-461.

3. Patankar, S.V.; and Spalding, D.B.: A Novel Finite Difference Formulation for Differential Expressions Involving both First and Second Derivatives. *Int. J. Numer. Methods Eng.*, vol 4, 1972, pp. 551-559.

4. Stone, H.L.; Iterative Solution of Implicit Approximation of Multidimensional Partial Differential Equations. *SIAM J. on Num. Analysis*, vol. 5, 1968, pp.530-558.

5. Khosla, P.K.; and Rubin, S.G.; A Diagonally Dominant Second-Order Accurate Implicit Scheme. *Computers and Fluids*, vol 2, 1974, pp.207-209.
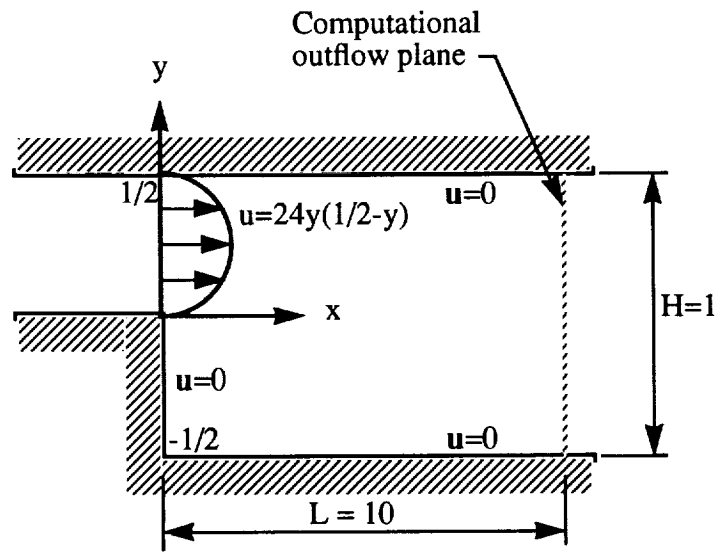
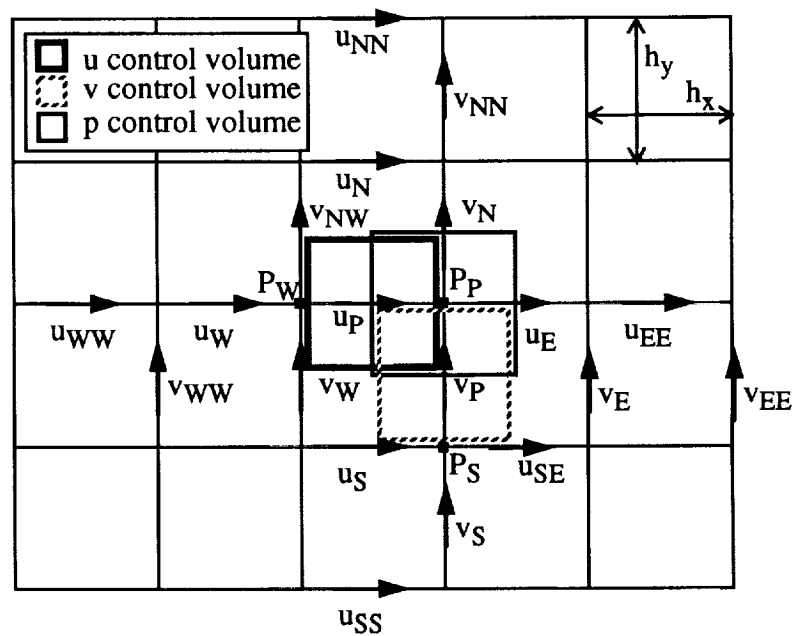Figure 1. Geometry and boundary conditions for flow over a backward facing step.

Figure 2. Location of variables for staggered grid.